Vehicle System Dynamics
Vol. 00, No. 00, Month 200x, 1–22

RESEARCH ARTICLE

Vehicle stability control using direct virtual sensors

M. Canale*,§ L. Fagiano§ ‡, F. Ruiz†, and M. C. Signorile§,
(*Received 00 Month 200x; final version received 00 Month 200x*)

The paper investigates the use of a Direct Virtual Sensor (DVS) to replace a physical sensor in a vehicle stability control system. A yaw control system is considered and the proposed solution can be particularly useful when a fault of the yaw rate physical sensor occurs. A DVS is a stable linear filter derived directly from input-output data, collected in a preliminary experiment. In this work it is shown that, by using data collected in a closed loop fashion, better DVS accuracy can be obtained with a reduced number of measured variables. Moreover, the robust stability of the closed loop system employing a DVS is studied. The effectiveness of the presented results is shown through numerical simulations of harsh maneuvers, performed using a detailed model of a vehicle equipped with an active front steering device.

Keywords: direct virtual sensor; vehicle stability; internal model control; robust control; fault tolerance

1. Introduction

Lateral stability control systems significantly enhance safety [1] and handling properties by modifying the dynamics of the passive vehicle. These systems usually employ a closed loop control strategy with a yaw rate feedback (see [2]). In particular, in this work a vehicle equipped with an active front steering (AFS) device is considered. Clearly, the yaw rate sensor plays a crucial role for the correct operation of the control system and sensor faults may lead to performance deterioration or even safety risks, unless a proper recovery strategy is adopted. In this context, virtual sensors can be employed to carry out a recovery strategy. Once the sensor fault has been detected, the measure of the yaw rate can be replaced by its estimate, provided by the virtual sensor.
Virtual sensors (see e.g. [3]) are software algorithms which exploit a set of available measurements to compute an estimate of a physical quantity of interest of a given plant. The common approach to derive a virtual sensor is to design a linear or nonlinear observer, based on a simplified plant model (see e.g. [4–6] in the case of yaw rate estimation). Linear observers like Kalman filters are simple to implement and they satisfy optimality properties provided that noise assumptions are met, but they are accurate only in a restricted range of operating conditions (see [7]). On the other hand, nonlinear observers may be able to give good estimates in a larger range of operating conditions, but their computational cost for on–line implementation may be high and stability of the estimation error is much harder to

* Corresponding author
§ Dipartimento di Automatica e Informatica, Politecnico di Torino, Italy.
‡ Department of Mechanical Engineering, University of California, Santa Barbara - CA, USA
† Departamento de Electrónica, Pontificia Universidad Javeriana, Colombia.
E-mail: massimo.canale@polito.it, lorenzo.fagiano@polito.it,
ruizf@javeriana.edu.co, mcarmela.signorile@polito.it

ISSN: 0042-3114 print/ISSN 1744-5159 online

DOI: 10.1080/0042311YYxxxxxxxx
http://www.informaworld.com

guarantee. Novel approaches to derive virtual sensors for linear and nonlinear systems have been recently introduced respectively in [8] and [9]. According to such methodologies, the virtual sensor is derived directly from suitable input–output data (i.e. Direct Virtual Sensor, DVS), collected in a preliminary experiment, in an open loop setting, using a one–step procedure which does not require the use of a model of the system (see e.g. [9]).
In this paper, the design of a linear yaw rate DVS and its use in feedback control will be studied. A quite extensive literature can be found regarding yaw rate estimation using the measures of wheel speeds (already available due to the presence of Anti–lock Braking Systems), steering angle (measured in electric power steering systems) and/or lateral acceleration see e.g. [4–6]. However, few works (see e.g. [10, 11]) investigate the use of combined yaw rate estimation and feedback for yaw control and none of them addresses the issue of guaranteeing closed loop system stability in the presence of virtual sensor. In this work, such issues are investigated. At first, the problem of how to make a suitable choice of the measured variables needed by the DVS is studied in order to enhance the estimation accuracy. It is shown that, using data collected in a closed loop fashion, better overall estimation performance can be obtained, with a reduced number of measured variables. The stability of the controlled system using the DVS is studied via an a posteriori robustness analysis. Finally, through simulations, the performance of the controlled vehicle is evaluated in critical conditions and when a recovery strategy is used in order to face a yaw rate sensor fault.
In the considered yaw control structure, the control action is generated through the superposition of a front steering angle by means of actuation devices like Active Front Steering (AFS, see e.g. [12]). Such a solution has been chosen for its safety properties since, contrary to steer by wire systems, the driver intervention on the steering angle is always kept by a mechanical link. The feedback controller design is carried out using a linear vehicle model and robust Internal Model Control (IMC, [13]) techniques based on H_∞ optimization, which have been already successfully applied in stability control problems [14–16]. The paper is organized as follows: in Section 2 the vehicle model employed for control design is described, while Section 3 summarizes the IMC design procedure when a physical yaw rate sensor is employed. The design procedure of the DVS and its use for vehicle yaw control are treated in Section 4. Finally, in Section 5, simulation results are presented and conclusions are given in Section 7.

2. Vehicle model

Vehicle stability control systems usually employ a feedback control structure where the controlled variable is the yaw rate $\dot{\psi}(t)$ and the controller is designed on the basis of a linear vehicle model. The control input is able to modify the vehicle dynamics by influencing the longitudinal and/or lateral tyre forces, using several physical mechanisms. Among the existing solutions (see e.g. [12, 15, 17–20]), in this paper an approach similar to AFS systems (see e.g. [12]) is adopted: the steering angle $\delta(t)$ of the front wheels is the sum of the contribution $\delta_d(t)$, issued by the driver via the conventional steering system, with the contribution $\delta_f(t)$, provided by the active system via an electromechanical device:

$$\delta(t) = \delta_d(t) + \delta_f(t) \tag{1}$$

Angle δ_d is related to the handwheel angle δ_v, provided by the driver, through the steering ratio τ, i.e. $\delta_d = \delta_v/\tau$. The value of $\delta_f(t)$ is restricted in the range $\pm 5^\circ$ due

to the actuator limitations in the considered AFS system. The adopted actuation solution is motivated by safety reasons, since the driver intervention on the front steering angle is always kept.
For the control design, a linear single track vehicle model is considered, assuming that angle δ(t) is the control input (see e.g. [2] for details). Under the typical assumptions for single track models, for a fixed vehicle speed $\overline{v}$ the following dynamic equilibria hold:

$$\begin{array}{l} a_y(t) = \overline{v}(\dot{\beta}(t) + \dot{\psi}(t)) = (F_{yf}(t) + F_{yr}(t))/m \\ J\ddot{\psi}(t) = aF_{yf}(t) - bF_{yr}(t) \end{array} \tag{2}$$

where m is the vehicle mass, J is the moment of inertia around the vertical axis, β is the side–slip angle, a and b are the distances between the center of gravity and the front and rear axles respectively and F_{yf} and F_{yr} are the front and rear axle lateral forces, respectively. The dynamic generation of tyre forces is also taken into account through the following first order equations:

$$\begin{array}{l} F_{yf}(t) + \frac{l_f}{\overline{v}}\dot{F}_{yf}(t) = -c_f\left(\beta(t) + a\frac{\dot{\psi}(t)}{\overline{v}} - \delta(t)\right) \\ F_{yr}(t) + \frac{l_r}{\overline{v}}\dot{F}_{yr}(t) = -c_r\left(\beta(t) - b\frac{\dot{\psi}(t)}{\overline{v}}\right) \end{array} \tag{3}$$

where l_f and l_r are the front and rear tyre relaxation lengths and the variables c_f and c_r stand for the front and rear axle cornering stiffnesses (see [21]).
In the presence of a physical yaw rate sensor, the measure of $\dot{\psi}(t)$ is employed for feedback control and the controller design is carried out on the basis of the transfer function $G_{\dot{\psi}}(s)$, between the steering angle $\delta(t)$ and the yaw rate $\dot{\psi}(t)$:

$$G_{\dot{\psi}}(s) = \frac{b_2 s^2 + b_1 s + b_0}{a_4 s^4 + a_3 s^3 + a_2 s^2 + a_1 s + a_0} \tag{4}$$

where

$$\begin{array}{l} a_4 = mJl_f l_r,\ a_3 = m\overline{v}J(l_f + l_r) \\ a_2 = J(m\overline{v}^2 + c_f l_r + c_r l_f) + m(c_f a^2 l_r + c_r b^2 l_f) \\ a_1 = \overline{v}(J(c_f + c_r) + m(c_f a(a - l_r) + c_r b(b + l_f))) \\ a_0 = c_f c_r l^2 - m\overline{v}^2(c_f a - c_r b) \\ b_2 = m\overline{v}ac_f l_r,\ b_1 = m\overline{v}^2 ac_f,\ b_0 = \overline{v}c_f c_r l \end{array} \tag{5}$$

Transfer function $G_{\dot{\psi}}(s)$ can be derived, for a fixed value of the speed $\overline{v}$, by applying the Laplace transform to equations (1)–(3). It is also useful to describe the relationships between the vehicle input δ and the lateral acceleration a_y, the difference between the angular speeds of the front wheels, $\Delta\omega_f$, and of the rear wheels, $\Delta\omega_r$. Such variables have been considered since their measures are either usually available on vehicles, due to the presence of electric power steering (EPS) and anti–lock braking (ABS) systems and thus they can be used as inputs for the yaw rate virtual sensor. Moreover, as a first approximation, under the same assumptions of the single track vehicle model, the values of $\Delta\omega_f(t)$ and $\Delta\omega_r(t)$ are related to $\dot{\psi}(t)$ through the following equations (see e.g. [2]):

$$\begin{array}{l} \Delta\omega_f(t) = \dot{\psi}(t)d_f/R_w \\ \Delta\omega_r(t) = \dot{\psi}(t)d_r/R_w \end{array} \tag{6}$$

where R_w is the nominal wheel radius (supposed to be the same for all of the four wheels) and d_f, d_r are the front and rear wheelbases respectively. Note that variables $\Delta\omega_f$ and $\Delta\omega_r$ are defined as:

$$\begin{aligned}\Delta\omega_f &= \omega_{f,h} - \omega_{f,v}\\ \Delta\omega_r &= \omega_{r,h} - \omega_{r,v}\end{aligned}$$

where ω denotes the wheel angular speed and the subscripts f, r, h, v stand for front, rear, right and left wheel position, respectively. On the basis of equations (1)–(6), transfer functions $G_{a_y}(s)$, $G_{\Delta\omega_f}(s)$ and $G_{\Delta\omega_r}(s)$ are derived, respectively between the input δ and the output variables a_y, $\Delta\omega_f$ and $\Delta\omega_r$:

$$\begin{aligned}G_{a_y}(s) &= \frac{c_3 s^3 + c_2 s^2 + c_1 s + c_0}{a_4 s^4 + a_3 s^3 + a_2 s^2 + a_1 s + a_0}\\ G_{\Delta\omega_f}(s) &= \frac{g_2 s^2 + g_1 s + g_0}{a_4 s^4 + a_3 s^3 + a_2 s^2 + a_1 s + a_0}\\ G_{\Delta\omega_r}(s) &= \frac{h_2 s^2 + h_1 s + h_0}{a_4 s^4 + a_3 s^3 + a_2 s^2 + a_1 s + a_0}\end{aligned} \tag{7}$$

where

$$\begin{aligned}&c_3 = Jl_r c_f \overline{v},\ c_2 = J\overline{v}^2 c_f,\ c_1 = \overline{v} blc_f c_r,\ c_0 = \overline{v}^2 c_f c_r l\\ &g_2 = m\overline{v} ac_f l_r d_f / R_w,\ g_1 = m\overline{v}^2 ac_f d_f / R_w\\ &g_0 = \overline{v} c_f c_r l d_f / R_w,\ h_2 = m\overline{v} ac_f l_r d_r / R_w\\ &h_1 = m\overline{v}^2 ac_f d_r / R_w,\ h_0 = \overline{v} c_f c_r l d_r / R_w\end{aligned} \tag{8}$$

3. Yaw stability control using a physical yaw rate sensor

In this Section, the adopted control structure is presented, together with its design procedure(Figure 2). The control objective is to track a reference yaw rate value $\dot{\psi}_{ref}(t)$, whose course is designed in order to improve the vehicle maneuverability, and to assist the driver in keeping directional stability under the different driving conditions. In particular, $\dot{\psi}_{ref}(t)$ is computed by means of a static map whose inputs are the handwheel angle $\delta_v(t)$, issued by the driver, and the vehicle speed $v(t)$. For given values of δ_v and $v(t)$, the map is designed so that the desired yaw rate is higher than the one obtained by the uncontrolled vehicle, thus obtaining a higher lateral acceleration value and narrower paths, i.e. better maneuverability. At the same time, the reference yaw rate map is designed in such a way that the related side-slip angle β is limited, so to improve directional stability. Finally, the map also takes into account the nonlinear behaviour of the vehicle as it approaches its lateral acceleration limit. The reference yaw rate map employed in this paper is shown in Figure 1. For a detailed description of the criteria followed in the map construction, the interested reader is referred to [14] and [16].
In the considered control structure, denoted as $(Q + \dot{\psi})$ in the following, the value of the control input $\delta_f(t)$ is the sum of a feedback contribution $\delta_{fb}(t)$ with a feedforward one $\delta_{ff}(t)$. The feedback controller is designed using IMC methodologies, since they have been proved to be effective in the context of robust vehicle stability control (see e.g. [14–16] for their application in different contexts).
The IMC controller $Q(s)$ is designed to optimize the vehicle performance, while guaranteeing robust stability in the presence of the model uncertainty induced by the wide range of operating conditions. In order to take into account such uncer-

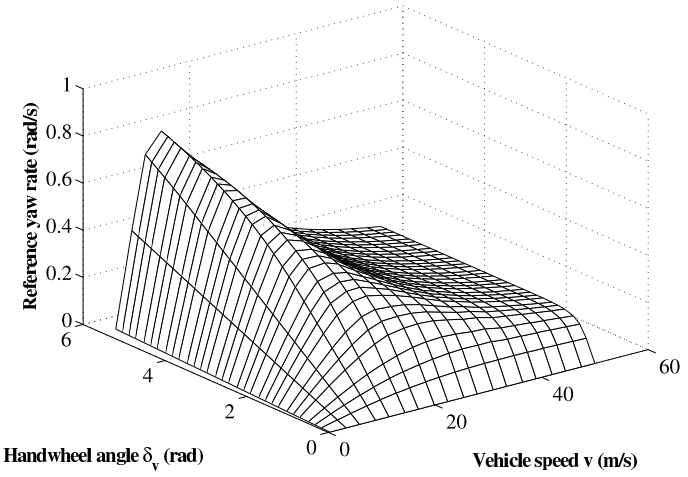

Figure 1. Yaw-rate reference map employed in the control system.

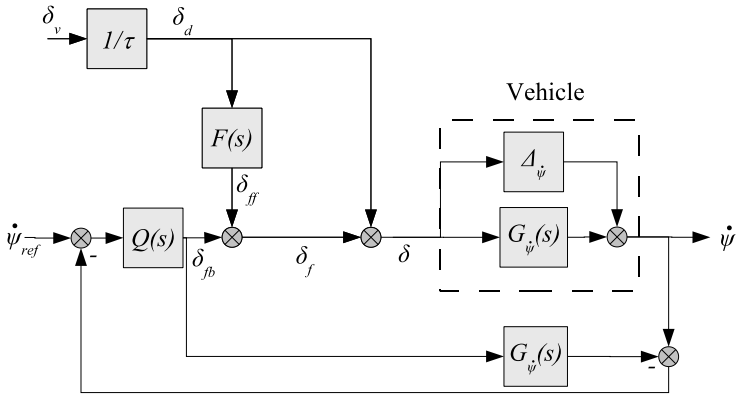

Figure 2. Control structure with measured yaw rate feedback and IMC controller $Q(s)$ ($Q + \dot{\psi}$).

tainty in the control design, an additive model set of the following form is employed:

$$\mathcal{G}_{\dot{\psi}}(G_{\dot{\psi}}, \Gamma_{\dot{\psi}}) = \{(G_{\dot{\psi}}(s) + \Delta_{\dot{\psi}}(s)) : |\Delta_{\dot{\psi}}(j\omega)| \leq \Gamma_{\dot{\psi}}(\omega)\} \tag{9}$$

$\Delta_{\dot{\psi}}(s)$ is the unstructured additive uncertainty (see e.g. [22]), while $\Gamma_{\dot{\psi}}(\omega)$ is an upper bound on the magnitude of $\Delta_{\dot{\psi}}(j\omega)$. Such model set can be obtained considering variations of the vehicle and tyre parameters with respect to their nominal values (see [22]), as described in Section 5. The design of $Q(s)$ is performed by means of the following optimization problem (see e.g. [13]):

$$Q(s) = \underset{\left\|Q(s)\bar{\Gamma}_{\dot{\psi}}(s)\right\|_\infty < 1}{\arg\min} \left\|W_S^{-1}(s)\, S(s)\right\|_\infty \tag{10}$$

where $\bar{\Gamma}_{\dot{\psi}}(s)$ is a suitable real rational stable function, whose magnitude strictly overbounds $\Gamma_{\dot{\psi}}(\omega)$ (9) and $W_S(s)$ is a weighting function which accounts for the desired performance on the nominal sensitivity $S(s) = 1 - G_{\dot{\psi}}(s)Q(s)$. $W_S(s)$ is chosen to achieve good closed loop damping properties and to slightly improve the system bandwidth with respect to the uncontrolled vehicle.
The feedforward contribution δ_{ff}, computed through the filter $F(s)$ from the measure of angle δ_d, issued by the driver, has been added to improve the dynamic response characteristic. In particular, the filter $F(s)$ is designed to match the de-

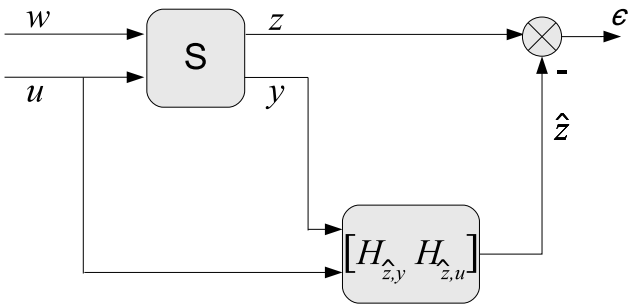

Figure 3. Process–virtual sensor scheme.

sired open loop yaw rate behavior, between the driver input δ_d and vehicle yaw rate $\dot{\psi}$, with the one described by an objective transfer function $T^{\text{des}}(s)$:

$$\dot{\psi}(s) = T^{\text{des}}(s)\delta_d(s) \tag{11}$$

According to the scheme in Figure 2, it results that

$$\begin{aligned} T^{\text{des}}(s)\delta_d(s) &= G_{\dot{\psi}}(s)\delta_d(s) + G_{\dot{\psi}}(s)\delta_{ff}(s) = \\ &= G_{\dot{\psi}}(s)\delta_d(s) + G_{\dot{\psi}}(s)F(s)\delta_d(s) \end{aligned}$$

thus the filter $F(s)$ can be computed as

$$F(s) = \frac{T^{\text{des}}(s)}{G_{\dot{\psi}}(s)} - 1 \tag{12}$$

Moreover, since $F(s)$ aims at enhancing the transient response only, its contribution should be deactivated in steady state conditions. This is achieved when the dc–gains of $T^{\text{des}}(s)$ and $G_{\dot{\psi}}(s)$ are equal.

4. Vehicle yaw control using DVS

4.1. *Virtual Sensors*

Let us consider a process $\mathcal{S}$ with a set of known inputs $u \in \mathbb{R}^m$, some unknown inputs (named disturbances) $w \in \mathbb{R}^r$, a set of measured outputs $y \in \mathbb{R}^q$ and an internal variable of interest $z \in \mathbb{R}$, to be estimated. A virtual sensor (see e.g. [3]) is a causal and stable dynamic system that takes as inputs the known inputs u and a subset of the measured outputs y of $\mathcal{S}$, and whose output is an estimate $\hat{z}$ of the internal variable $z \in \mathbb{R}$. In the linear case, the virtual sensor dynamic behavior can be described as:

$$\hat{Z}(s) = H_{\hat{z},y}(s)Y(s) + H_{\hat{z},u}(s)U(s) \tag{13}$$

where $H_{\hat{z},u}(s)$ and $H_{\hat{z},y}(s)$ are real rational stable transfer matrices of suitable dimension. Figure 3 shows the general process–virtual sensor scheme together with the approximation error ϵ. Different methodologies can be employed to build a virtual sensor, according to the considered prior information and assumptions. The most common techniques rely on the use of a (usually linear) process model and particular hypotheses about disturbances. Some of these approaches are the minimum variance (Kalman) and $\mathcal{H}_\infty$ filtering techniques. With these techniques, the

obtained estimation accuracy may be poor due to neglected dynamics in the employed model and due to the presence of (often uncertain) nonlinear characteristics in the real process (see [9]).

4.2. *Direct virtual sensors*

When the process is not completely known, a data–driven approach to the virtual sensor design problem can be considered. In this paper, a direct procedure is followed, in which suitable process input–output experimental data are used to design a DVS in one step, avoiding the identification of a model of the process. A preliminary experiment can be performed also when the variable z is measured. This assumption is not restrictive, since some measurements of z are needed to evaluate the performance of any virtual sensor, independently on the employed design methodology. Moreover, in the considered automotive context, extensive experimental testing campaigns are usually carried out, in order to tune the control algorithms and to assess the active system performance. During such experimental tests, in order to collect large quantities of data, the employed prototype car is equipped with a full set of sensors that, usually, are not all installed on the final commercialized vehicle due to their excessive costs.
Denote with u_k, y_k and z_k the sampled values of u, y and z respectively, corresponding to any sampling instant $k \in \mathbb{N}$, with fixed sampling period T_s. N measurements of u_k, y_k and z_k, corresponding to sampling instants $k\,T_s$, $\forall k \in [1, N]$, are collected in the preliminary experiment. In the following, the values of u_k, y_k, z_k, $k = 1, ..., N$, are referred to as the "data set". Since a virtual sensor must be a stable system, its impulse response has an exponential decay and it can be approximated with desired precision by a Finite Impulse Response (FIR) filter that uses present and past values of u_k and y_k to give an estimate $\hat{z}_k$ of z_k, that is:

$$\hat{z}_k = \sum_{j=0}^{n_u} \alpha_j^T u_{k-j} + \sum_{j=0}^{n_y} \beta_j^T y_{k-j} \tag{14}$$

where n_u, n_y are design parameters which define the structure of the DVS and $\alpha_j \in \mathbb{R}^m$, $j = 0, \ldots, n_u$ and $\beta_j \in \mathbb{R}^q$, $j = 0, \ldots, n_y$ are the filter coefficients, whose values are constrained by the following exponential decay:

$$\|\alpha_j\|_\infty \leq L_u \rho^j,\ j \in [0, 1, \ldots, n_u]$$
$$\|\beta_j\|_\infty \leq L_y \rho^j,\ j \in [0, 1, \ldots, n_y]$$

where $L_u > 0$, $L_y > 0$ and $0 < \rho < 1$. L_u, L_y and ρ are the parameters that define the model class where the DVS is looked for. In particular, L_u and L_y define the maximum absolute value of any one of the elements of the first coefficients in the impulse response (i.e. α_0 and β_0), while ρ is the decay rate.
Assuming that z is observable from y, it can be shown that the estimation error $\epsilon_k = z_k - \hat{z}_k$ is bounded for any bounded input sequence (see [8]). Using FIR filters with the structure (14), the DVS can be designed by minimizing a weighted p–norm of the estimation error on the collected data set, i.e. on the collected values of u_k, y_k and z_k for any $k \in [\underline{k}, N]$, where $\underline{k} = \max(n_u, n_y)$:

Table 1. Subsets of measurements used for the DVS design

DVS	Measurements
1	$[\delta, a_y]$
2	$[\delta, \Delta\omega_f]$
3	$[\delta, \Delta\omega_r]$
4	$[\delta, a_y, \Delta\omega_f]$
5	$[\delta, a_y, \Delta\omega_r]$
6	$[\delta, \Delta\omega_f, \Delta\omega_r]$
7	$[\delta, a_y, \Delta\omega_f, \Delta\omega_r]$

$$
\begin{aligned}
&[\hat{\alpha}_0, \ldots, \hat{\alpha}_{n_u}, \hat{\beta}_0, \ldots, \hat{\beta}_{n_y}] = \arg\min \left(\sum_{k=\underline{k}}^{N} \left| \mathrm{w}_k^{-1} \epsilon_k \right|^p \right)^{1/p} \\
&\qquad \text{such that} \\
&\begin{cases}
\epsilon_k = z_k - \sum_{j=0}^{n_u} \alpha_j u_{k-j} - \sum_{j=0}^{n_y} \beta_j y_{k-j} \quad k \in [\underline{k}, N] \\
\|\alpha_j\|_\infty \leq L_u \rho^j, \ j \in [0, 1, \ldots, n_u] \\
\|\beta_j\|_\infty \leq L_y \rho^j, \ j \in [0, 1, \ldots, n_y]
\end{cases}
\end{aligned} \tag{15}
$$

This convex optimization problem with linear constraints can be efficiently solved. By suitably selecting the weights w_k in (15), it is possible to consider noise measures dependent on k, for example relative measurement errors. Details on how to select the exponential decay parameters L_u, L_y and ρ and weights $\mathrm{w_k}$ are given in [23].

Depending on the data set employed in the design, the obtained linear DVS is able to give good estimation performance also in nonlinear process operating conditions, when the linear models used in classic approaches suffer from under–modeling (for a complete comparison, see [8]).

Regardless of the used norm, solution to problem (15) is usually a high order FIR filter. Then, model order reduction techniques are used to fit the identified impulse responses with a stable and causal IIR filter of a prefixed order n. An n-th order state-space realization is obtained by singular value decomposition of the Hankel matrix of the filter impulse response, such that the H_∞ distance between the original and the low order filter is bounded, see [24]. Finally, a bilinear transformation is applied to the resulting estimator in order to obtain the form (13).

4.3. *DVS for yaw rate*

The design and the use of a yaw rate DVS for feedback control is now studied. Thus, referring to Section 4.2, the variable z to be estimated is the yaw rate $\dot{\psi}$, while the variable u is the front steering angle, i.e. $u = \delta$. As to variable y, it is assumed that the measures of the lateral acceleration a_y and of the differences between the wheel angular speeds of the front and rear axles, $\Delta\omega_f$ and $\Delta\omega_r$ respectively, are available. Therefore, the considered output y is composed of a suitable subset of the variables a_y, $\Delta\omega_f$ and $\Delta\omega_r$. Table 1 lists all the possible virtual sensors.

By intuition, it could be expected that the best estimation accuracy can be obtained when all of the possible available measurements are used. However, an interesting outcome of this paper is that this is not true in general, since the use of all of the three measures of a_y, $\Delta\omega_f$ and $\Delta\omega_r$ does not always lead to the best accuracy results. In particular, it will be shown that, if the initial experiment is performed in closed loop fashion, the DVS which achieves the best accuracy employs the measures of a_y and $\Delta\omega_r$ only. Moreover, such DVS has better accuracy than those

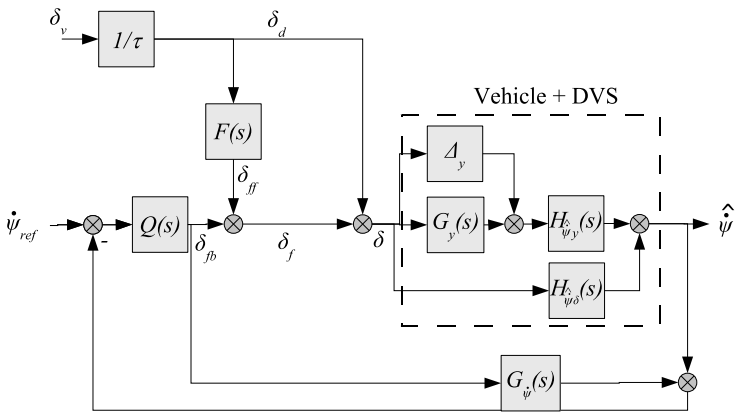

Figure 4. Control structure with estimated yaw rate feedback and IMC controller $Q(s)$ $(Q + DVS)$.

designed using data collected with the uncontrolled vehicle, independently on the number of employed measurements. However, figuring out a priori which measured variables should be used to obtain good accuracy appears to be a hard task: physical insight and trial–and–error procedures can be used to practically establish the best combination of measurements to be employed.

4.4. *Yaw control using DVS*

Closed loop stability when the DVS is used for feedback control is now investigated. Figure 4 shows the considered control scheme where the yaw rate DVS replaces the physical one, e.g. to recover the yaw rate sensor fault. This scheme is denoted $(Q + DVS)$ for brevity. Since the estimated variable $\hat{z}$ is the yaw rate $\widehat{\dot{\psi}}$ and the input u is the steering angle δ, the transfer matrices of the DVS (see (13))are denoted with $H_{\widehat{\dot{\psi}},y}$ and $H_{\widehat{\dot{\psi}},\delta}$. A sufficient robust stability condition, based on the small gain theorem (see e.g. [22]), is employed to assess if the controller $Q(s)$ is still able to robustly stabilize the system in the presence of the DVS. To this end, the nominal transfer matrix $G_y(s)$, from input δ to the considered output y, is computed. $G_y(s)$ is a single–column transfer matrix whose components are one or more of the transfer functions (7), depending on the particular considered variable y. For example, the transfer matrix $G_y(s)$ related to DVS 4 (see Table 1 and (7)) is defined as:

$$G_y(s) = \begin{bmatrix} G_{a_y}(s) \\ G_{\Delta\omega_f}(s) \end{bmatrix}$$

Model uncertainty is taken into account by the following additive model set:

$$\mathcal{G}_y(G_y, \Gamma_y) = \{G_y(s) + \Delta_y(s) : \bar{\sigma}\left(\Delta_y(j\omega)\right) \leq \Gamma_y(\omega)\} \tag{16}$$

where $\bar{\sigma}(\cdot)$ is the maximum singular value and $\Delta_y(s)$ is the transfer matrix of the additive uncertainty associated to $G_y(s)$, while $\Gamma_y(\omega)$ is an upper bound of $\bar{\sigma}\left(\Delta_y(j\omega)\right)$, which can be computed by considering variations of the vehicle and tyre parameters with respect to their nominal values (as described e.g. in [22]).

Table 2. Vehicle model parameters

Model parameters	Values
m	1715 kg
$\overline{v}$	100 km/h
J	2697 kgm^2
a	1.07 m
b	1.47 m
l_f	1 m
l_r	1 m
c_f	89733 Nm/rad
c_r	114100 Nm/rad
R_w	0.303 m
d_f	1.48 m
d_r	1.35 m
τ	15.4

Referring to Figure 4 and defining the functions:

$$G_{DVS}(s) = H_{\hat{\dot{\psi}},y}(s)G_y(s) + H_{\hat{\dot{\psi}},\delta}(s)$$
$$\Delta_{DVS}(s) = H_{\hat{\dot{\psi}},y}(s)\Delta_y(s)$$
$$C(s) = Q(s)(1 - G_{\dot{\psi}}(s)Q(s))^{-1}$$

the following sufficient condition can be used to check robust stability of control scheme $(Q + DVS)$.

Robust stability of control scheme $(Q + DVS)$

The control scheme $(Q + DVS)$ is robustly stable with respect to the model uncertainty Δ_y in the model set (16) if

$$\left\|\Gamma_{DVS}(s)C(s)(1 + C(s)G_{DVS}(s))^{-1}\right\|_\infty < 1 \tag{17}$$

where $\Gamma_{DVS}(s)$ is a stable real rational transfer function, such that

$$\bar{\sigma}\left(\Delta_{DVS}(j\omega)\right) \leq |\Gamma_{DVS}(j\omega)|$$

Proof. $C(s)$ is the equivalent feedback controller of the IMC loop formed by $Q(s)$ and $G_{\dot{\psi}}(s)$, $G_{DVS}(s)$ is the nominal transfer function from δ to $\hat{\dot{\psi}}$ and $\Delta_{DVS}(s)$ is the resulting additive uncertainty of $G_{DVS}(s)$. Equation (17) follows from the application of the small gain theorem to the equivalent feedback loop with additive uncertainty. ■

5. Simulation results

5.1. *Controller design*

The IMC design has been performed using transfer function $G_{\dot{\psi}}(s)$ (see (4)) and vehicle parameter values as shown in Table 2. Model sets (9) and (16) have been obtained by considering variations of the vehicle nominal speed between 70 and 130 km/h, independent variations of rear and front tyre cornering stiffness between [-30%, +10%], increments of vehicle mass up to +20% distributed as 30% on the front axle and 70% on the rear axle, with the consequent changes of distances between the center of gravity and the front and rear axles and of moment of inertia. Moreover, a variation of ±10% of the tyre radius has been considered too. The

control input δ_f is supposed to be mechanically limited such that $|\delta_f| \leq 5°$.
The IMC controller $Q(s)$ has been obtained as the solution of (10), using the following weighting function:

$$W_S(s) = 1.06\frac{s}{s+5} \tag{18}$$

The feedforward filter $F(s)$ in (12) has been computed using the following transfer function $T^{\text{des}}(s)$:

$$T^{\text{des}}(s) = \frac{4.488}{(1+s/20)^2}.$$

Functions $W_S(s)$ and $T^{\text{des}}(s)$ have been chosen and tuned in order to achieve a good compromise between steady state behavior and closed loop specifications. In particular, for $W_S(s)$, a zero at the origin has been employed to ensure servo performance, so that in steady-state conditions the reference yaw rate, which has been chosen in order to improve vehicle maneuverability, is attained with zero tracking error. The gain and the pole of $W_S(s)$ have been chosen to impose a limited resonance peak and larger bandwidth with respect to the uncontrolled vehicle, so to improve the damping of the vehicle transient response and reduce the response time, thus enhancing the vehicle handling performance.

5.2. *Direct virtual sensors design and performance*

A 14 d.o.f. nonlinear vehicle model has been used to generate the data sets required for the design and the validation of the virtual sensors. Nonlinear characteristics obtained on the basis of measurements on a real vehicle have been employed to model the tyre, steer and suspension behavior. A first-order dynamical model of each wheel has been used to compute the wheel speed. The employed tyre model, described e.g. in [21], takes into account the interaction between longitudinal and lateral slip, as well as vertical tyre load and suspension motion, to compute the tyre longitudinal and lateral forces and self–aligning moments. An example of the employed tyre friction ellipses is shown in Figure 5, where the lateral friction coefficient is reported as a function of the exploited longitudinal friction (during traction) and of the tyre slip angle α.

Figure 6 shows a comparison between the yaw rate measured on the real vehicle during a track test, and the one obtained in simulation with the considered model. Using such detailed 14 d.o.f. vehicle model, two data sets have been obtained through two different experiments, lasting 90 s each. In both experiments, the vehicle speed is kept constant at 70 km/h during the first 25 s, then it is gradually increased up to 100 km/h at 35 s, from 35 s to 55 s it is kept at 100 km/h, in the next 10 s the speed is gradually increased up to 130 km/h and maintained at this value for the last 25 s.
In the first experiment, the vehicle has been driven in open loop, by imposing a suitably designed course $\delta_d^{\text{id}}(t)$ of δ_d, composed of quick ramps and constant intervals plus a pseudo–random binary signal. The second experiment has been performed in closed loop fashion using the control scheme $(Q + \dot{\psi})$. In this case, the vehicle is driven by means of the same driver input $\delta_d^{\text{id}}(t)$ and employing the controller $Q(s)$ and the filter $F(s)$ designed as described in Section 3 and 5.1.
Seven DVS have been designed for each data set, considering all possible combination of the available measurements (see Table 1). Each DVS has been identified by solving the optimization problem (15) using either the open or the closed loop data

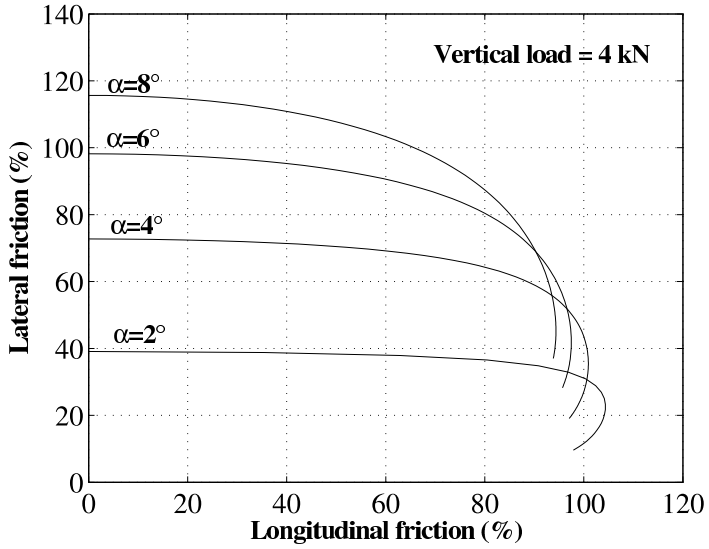

Figure 5. Front tyre friction ellipses considered in the 14 degrees of freedom model, with different values of lateral slip angle α, for a constant vertical load of 4 kN.

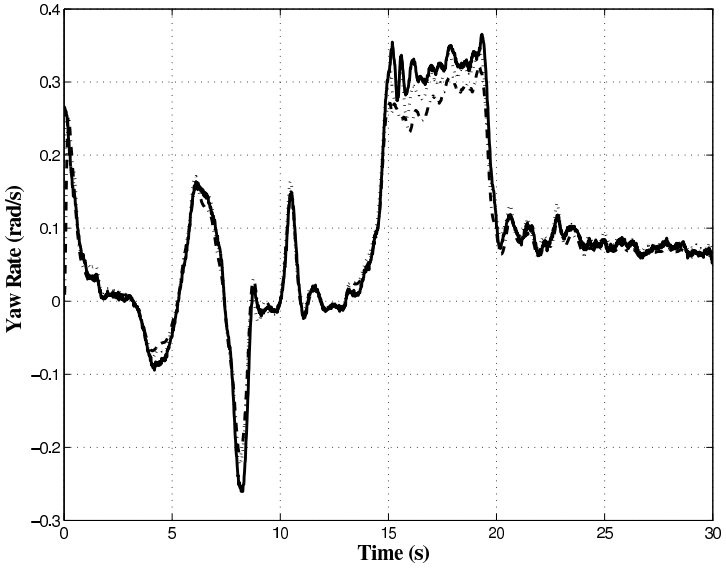

Figure 6. Comparison between the measured yaw rate (solid) during a track test on the real vehicle, the simulated yaw rate obtained with the 14 d.o.f. model (dotted) and the estimate provided by the DVS (dash-dotted).

set, for $p = 2$ and unitary weights, i.e. the resulting filter is the FIR model that minimizes the sum of squared errors, while having an impulse response bounded by the decay rate defined by L and ρ.

Different bounds on the decay rate have been considered for each DVS, adjusting the filter lengths accordingly, and the ones giving the lowest estimation error, while satisfying the robust stability condition (17), have been selected. Table 3 shows the length $n_{FIR} = n_u = n_y$ and decay rate constraints $L = L_u = L_y$ and ρ of the designed DVSs, and the order n of the corresponding virtual sensors obtained after the order reduction step.

In order to evaluate the control system performance when the yaw rate estimate $\widehat{\dot{\psi}}$ given by the DVS is used, simulations have been performed employing the 14 d.o.f. nonlinear vehicle model and the control structure $(Q + DVS)$. In particular,

Table 3. Parameters for DVS design

DVS	L	ρ	n_{FIR}	n
1	0.4	0.96	150	10
2	0.3	0.92	100	8
3	0.3	0.92	100	8
4	0.6	0.92	100	8
5	0.6	0.90	100	10
6	0.3	0.95	150	8
7	0.3	0.95	150	10

the following maneuvers have been considered:

- constant speed steering pad at 100 km/h: the handwheel angle is increased slowly (1°/s) to evaluate the steady state tracking behavior
- steer reversal test with handwheel angle of 5° and 50°, at 90 km/h, to evaluate steady state and transient vehicle performance in linear and nonlinear operating conditions.

Table 4 shows the obtained accuracy results for the steering pad tests, in terms of maximum relative estimation error $\hat{E}_{\max}$ and mean relative estimation error $\hat{E}_{\text{mean}}$:

$$\hat{E}_{\max} = \max_{t\in[t_0,t_{end}]} \hat{e}(t) \tag{19}$$

$$\hat{E}_{\text{mean}} = \frac{1}{t_{end}-t_0}\int_{t_0}^{t_{end}} \hat{e}(t)dt \tag{20}$$

where

$$\hat{e}(t) = \left|\frac{\hat{\dot{\psi}}(t)-\dot{\psi}(t)}{\dot{\psi}(t)}\right|,\ \dot{\psi}(t)\neq 0$$

and t_0, t_{end} are the starting and final test time instants respectively. Since the steering pad is a steady state maneuver, the values of $\hat{E}_{\max}$ and $\hat{E}_{\text{mean}}$ can be considered as measures of the static DVS performance.

The results presented in Table 4 show that a bounded estimation error is obtained

Table 4. Steering pad test using DVS

	Open loop		Closed loop	
DVS	$\hat{E}_{\max}$	$\hat{E}_{\text{mean}}$	$\hat{E}_{\max}$	$\hat{E}_{\text{mean}}$
1	34.9%	24.8%	43.8%	30.8%
2	22.4%	14.3%	16.2%	9.3%
3	24.5%	16.2%	17.3%	9.7%
4	19.8%	13.4%	12.8%	8.5%
5	20.6%	13.6%	**12.2%**	**6.9%**
6	20.0%	9.5%	19.6%	13.2%
7	**14.7**%	**7.1**%	13.3%	8.2%

with all the considered virtual sensors. DVS 1, which employs the measure of $a_y(t)$ only, gives the worst performance, while all of the other filters show similar estimation errors. In most cases, the use of closed loop data gives better results than using open loop data.

Table 5. 5° steer reversal test using DVS

	Open loop		Closed loop	
DVS	$\hat{E}_{\text{mean}}$	E_{mean}	$\hat{E}_{\text{mean}}$	E_{mean}
1	37.1%	37.2%	33.7%	29.8%
2	31.3%	24.6%	20.4%	16.0%
3	33.0%	25.2%	20.9%	16.2%
4	21.9%	21.6%	16.4%	**13.5%**
5	24.8%	23.2%	**16.0%**	13.9%
6	23.2%	17.3%	24.2%	18.7%
7	**21.2**%	**17.8**%	**16.0%**	14.0%

Table 6. 50° steer reversal test using DVS

	Open loop		Closed loop	
DVS	$\hat{E}_{\text{mean}}$	E_{mean}	$\hat{E}_{\text{mean}}$	E_{mean}
1	20.0%	22.4%	16.4%	12.6%
2	12.5%	8.4%	9.0%	4.7%
3	13.2%	10.6%	8.6%	5.0%
4	12.3%	10.8%	8.6%	5.1%
5	9.5%	15.4%	**6.8%**	**2.8%**
6	**8.4**%	**4.4**%	8.4%	4.8%
7	10.3%	6.2%	7.2%	3.2%

Tables 5 and 6 show the obtained performance in the steer reversal tests in terms of the index $\hat{E}_{\text{mean}}$ (20) and of the mean relative tracking error E_{mean}:

$$E_{\text{mean}} = \frac{1}{t_{end} - t_0} \int_{t_0}^{t_{end}} e_{ref}(t) dt \tag{21}$$

where

$$e_{ref}(t) = \left| \frac{\dot{\psi}_{ref}(t) - \dot{\psi}(t)}{\dot{\psi}_{ref}(t)} \right|, \; \dot{\psi}_{ref}(t) \neq 0$$

Note that virtual sensors identified from closed loop data perform better than those identified from open loop data, especially in the 50° steer reversal maneuver. This is due to the fact that, in the presence of the control action, the closed loop vehicle transient response is different from the open loop one. Thus, by using closed loop experimental data a more appropriate information about the process is taken into account in the DVS design.

Moreover, it can be noted (see Tables 4–6, bold–faced text) that the best overall estimation accuracy is given by DVS 5, obtained using the closed loop data set and the measures of $a_y(t)$ and $\Delta\omega_r(t)$ only, which performs better than DVS 7 that exploits all of the possible available measurements, designed either using the closed loop or the open loop data sets. It is not trivial to explain, from the practical point of view, why such a result has been obtained. From a theoretical point of view, the signals with higher correlation with the estimated variables are those that give more information and that should be employed. This is surely the case, in this particular application, of the lateral acceleration, as it is intuitive and also evident by the poor results achieved by DVSs n. 2, 3 and 6, and of at least one of the two wheel speed differentials, since DVS 1 (that does not employ the measure of wheel speed difference) also has bad performance. The remaining DVSs n. 4, 5 and 7 have very similar estimation accuracy. The employed vehicle is an all-wheel drive one, so that wheel slip during traction is present on all wheels, which may explain why the results of DVSs 4,5 and 7 (closed-loop) are so close one to the

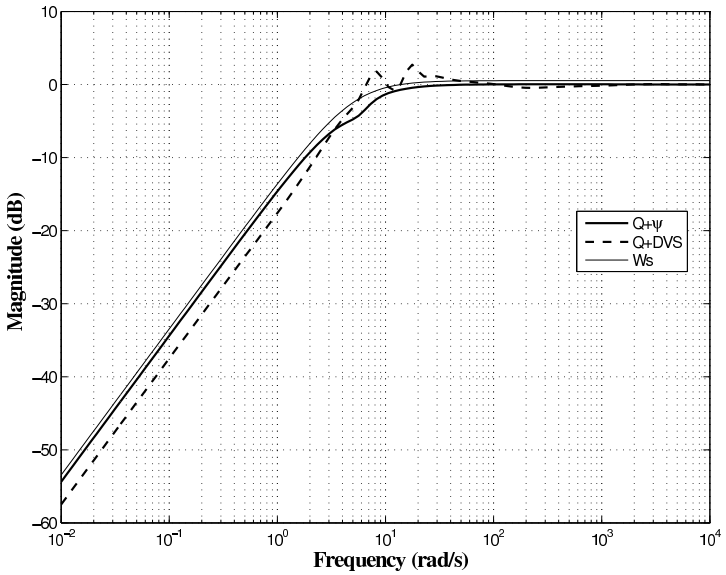

Figure 7. Thin solid line: weighting function W_S. Sensitivity functions of the control scheme $(Q + \dot{\psi})$ (solid), $(Q + DVS)$ (dashed).

other. With a 2-wheel drive vehicle, one would expect the non-driven wheel speeds to give a more accurate yaw-rate estimate.
Finally, the accuracy of the DVS 5 has been evaluated on experimental data measured on the real vehicle during a track test with vehicle speed varying between 50 km/h and 120 km/h and lateral acceleration up to 7.5 m/s^2. In Figure 6, the estimate provided by DVS 5 is compared to the yaw rate measured during a track test and to the yaw rate course obtained with the 14 d.o.f. vehicle model. The mean relative error between the measured yaw rate and the simulated one is 8.6%, while the mean relative error between the measured yaw rate and the one given by DVS 5 is 13%.

5.3. *Vehicle performance using a direct virtual sensor for feedback control*

According to the results reported in Tables 4–6, DVS 5, identified from closed loop data, has been chosen to compare performance of the control structures $(Q + \dot{\psi})$ and $(Q + DVS)$ which use, respectively, the measured and estimated yaw rate. In Figure 7, sensitivity functions of the considered control schemes are compared with the desired sensitivity described by the weighting function $W_S(s)$ (18). It can be noted that the magnitude course of sensitivity functions related to the scheme $(Q+\dot{\psi})$ satisfies the nominal performance. Although the magnitude of the nominal sensitivity of the closed loop system $(Q + DVS)$ shows a higher peak value, it has a greater noise attenuation level at low frequencies.
In order to assess the behaviour of the control systems when a DVS is employed for feedback and to analyze the results of the recovery strategy when a fault of the yaw rate sensor occurs, the following simulation tests have been performed:

- 50° steer reversal maneuver performed on dry road with vehicle speed varying between 50 km/h and 120 km/h. This test aims to assess the robustness of the control system both in the absence and in the presence of DVS, in different operating conditions.
- brake–in–a–turn test performed at 110 km/h with handwheel angle of 15° and a braking action of $0.5g$ (g is the gravitational acceleration). The braking occurs when the transient phase of the step steer has been finished and lasts 3 s, from

the 5^{th} until the 8^{th} second of the maneuver. Note that during this maneuver the vehicle is subject to significant lateral acceleration and non constant longitudinal speed (from 110 to 50 km/h) due to the sudden braking, thus making this a quite demanding robustness test. The maneuver has been also performed when a fault of the yaw rate sensor occurs after 7 s from the beginning.

- ISO double lane change maneuver as reported in [21]. This maneuver has been performed once on wet road with constant speed $v_{\text{ref}} = 100\,\text{km/h}$ and with vehicle mass increased by +200 kg and then on iced road, with constant speed $v_{\text{ref}} = 50\,\text{km/h}$ in a fault recovery situation. After 6 s from the start of the maneuver, a fault of the yaw rate sensor occurs and the measure of the yaw rate is replaced by its estimate provided by the DVS. The following driver's model has been used:

$$\tau_d \dot{\delta}_v(t) + \delta_v(t) = K_d \left(\psi_{\text{ref}}(t) - \psi(t)\right) \tag{22}$$

where $\psi_{\text{ref}}(t)$ is the course of the reference yaw angle, corresponding to the ISO double lane change path at the considered speed (see [21]), and K_d, τ_d are the driver gain and the driver time constant respectively. Although more complex driver models could be employed (see e.g. [21]), the simple model (22) has been considered in this work because the purpose here is to make a comparison between the behavior of the uncontrolled vehicle and of the controlled ones, given the same driver model, rather than to use a detailed driver model. As regards the driver's model parameters, the values $K_d = 10.8$ and $\tau_d = 0.2\,\text{s}$ have been considered. Note that the values of τ_d roughly range from 0.08 s (experienced driver) to 0.25 s (unexperienced driver), while the higher is the driver gain, the more aggressive is the driving action which could more likely cause vehicle instability.

Figure 8 shows the variation of time responses of the controlled vehicle with physical sensor and DVS in terms of normalized yaw rate $\dot{\psi}(t)/\dot{\psi}_{ref}(t)$. As expected, the vehicle using the measured yaw rate shows better performance both in transient and steady state however robust stability is achieved in both cases. It can be noted that the DVS tends to underestimate the vehicle yaw rate, so that the actual yaw rate results to be higher than the reference one (see Figure 8, bottom), thus bringing the vehicle closer to its lateral acceleration limit. This issue can be circumvented both by designing a reference yaw rate map that takes into account the potential estimation errors of the DVS (i.e. leaving some "margin" between the reference yaw rate and the limits of handling) and by alerting the driver, in case of sensor fault, through suitable warning lights and/or sounds that notify that the yaw control systems is running in recovery regime, so to induce a more cautious driving behavior.

Figure 9 shows the results of the brake–in–a–turn maneuver. The results of this test indicate that the designed yaw control system is able to effectively intervene when the vehicle is driven in a turn at high speed and significant braking forces occur. Note that such a test is quite demanding for the considered control system, since braking forces have not been considered neither in the control design (based on a LTI single track model), nor in the DVS design (since no such maneuvers have been included in the data set collected in the preliminary experiments). Moreover, from Figure 9.a it can be noted that while the passive vehicle is stable, the controlled one becomes unstable when a fault of the yaw rate sensor occurs and it is not recovered, see Figure 9.b. In fact, since no yaw rate measure is provided in feedback, the control loop is open. On the other hand, recovery of the fault is allowed when the DVS gets on duty ensuring stability and acceptable performance on the controlled system.

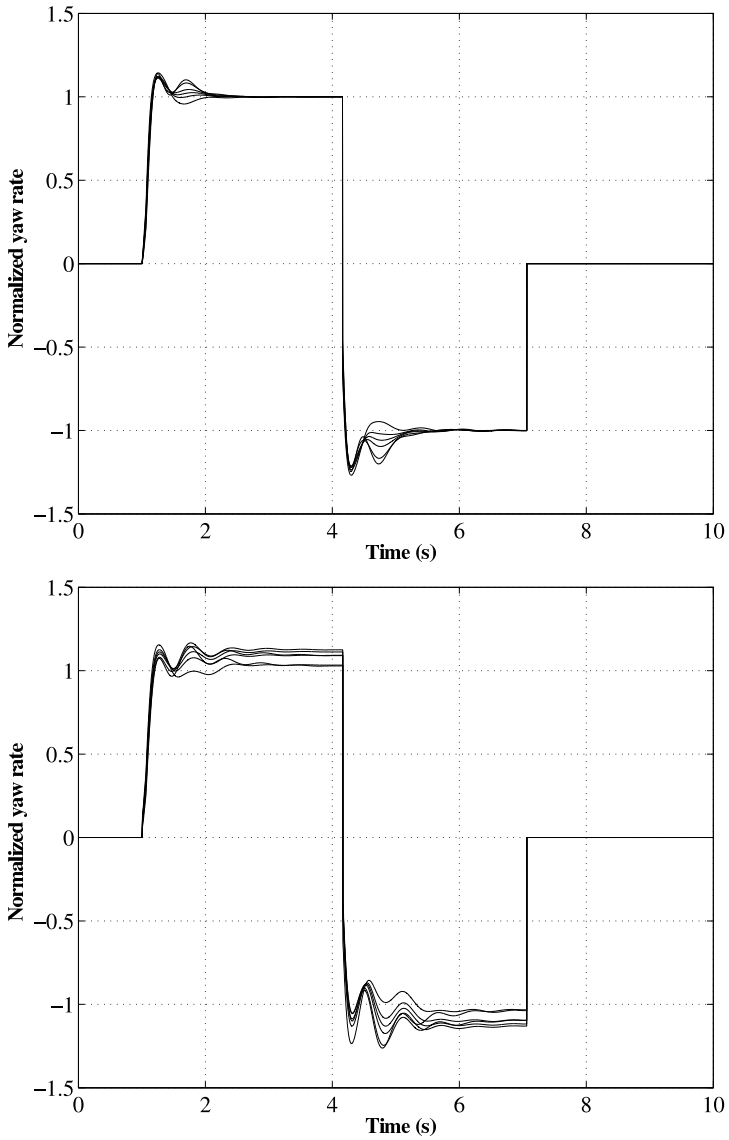

Figure 8. Steer reversal test with handwheel angle value of 50°, performed with varying vehicle speed between 50 km/h and 120km/h. Courses of the normalized yaw rate $\dot{\psi}(t)/\dot{\psi}_{ref}(t)$ of the vehicle controlled with $(Q + \dot{\psi})$ (top) and with $(Q + DVS)$(bottom).

Figures 10–11 show the results obtained in the ISO double lane change maneuver on wet road, in absence of fault, when the vehicle mass is increased of 200 kg. It can be noted that the uncontrolled vehicle shows excessive oversteering and instability in the last part of the maneuver. On the other hand the controlled vehicles (i.e. using the $(Q + \dot{\psi})$ and $(Q + DVS)$ schemes) are able to successfully complete the test giving a further evidence of the robustness properties of $Q + DVS$ structure. Note that, as shown in Figure 10, a lateral acceleration value of about 7.3 m/s^2, corresponding to about 95% of the maximal vehicle lateral acceleration, is reached by the vehicles controlled using the schemes $(Q + DVS)$. Thus, the results of this test indicate that the designed yaw control system is able to effectively aid the driver, also when the DVS is used instead of a physical sensor, despite the presence of driver's feedback, wet road and increased mass, that were not considered in the preliminary experiments performed to collect the data for the DVS identification. Figures 12–13 show the results obtained with the ISO double lane change maneuver on iced road when the yaw rate sensor fault occurs. It can be noted that the

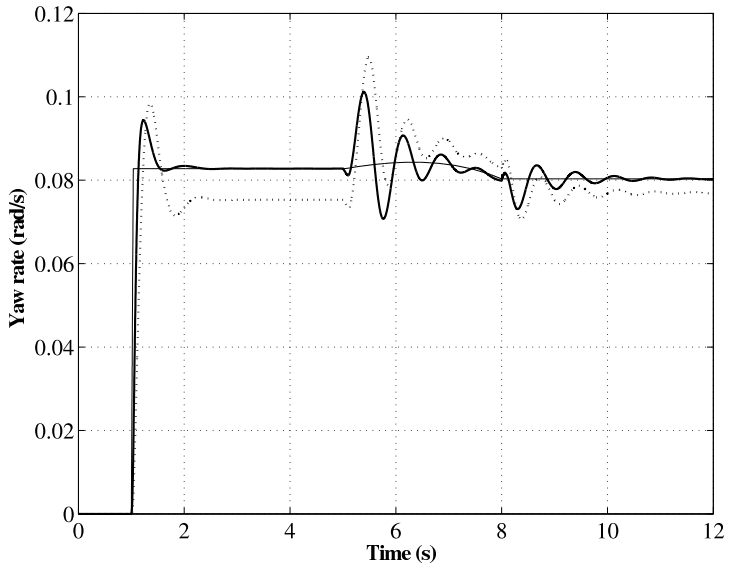

(a)

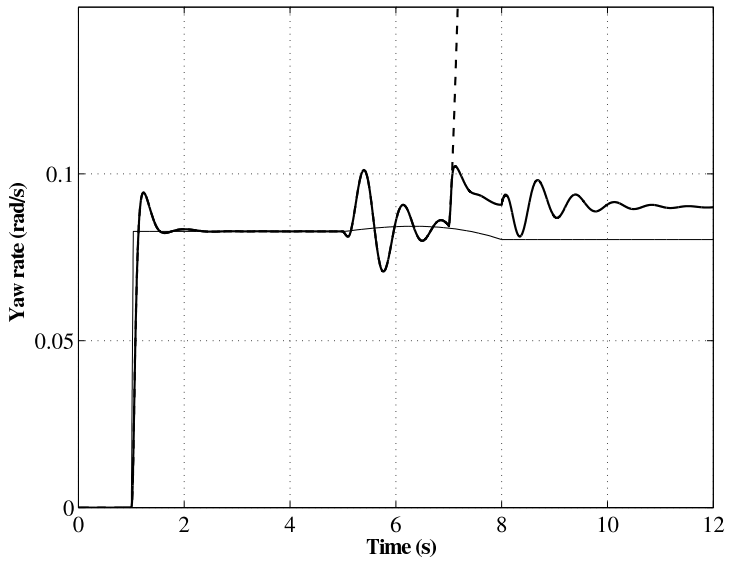

(b)

Figure 9. Brake in a turn test at 110 km/h with 15° handwheel angle and deceleration of 0.5g. Thin line: reference yaw rate. (a) Dotted line: uncontrolled vehicle, solid: vehicle controlled with (Q + $\dot{\psi}$). (b) Solid: vehicle controlled with (Q + $\dot{\psi}$) until 7 s when the sensor fault occurs and then with (Q + DVS). Dashed: vehicle controlled with (Q + $\dot{\psi}$) until 7 s and then it remains in open loop.

uncontrolled vehicle is unstable in the last part of the maneuver, while the controlled ones are able to successfully complete the test. In particular, the controlled vehicle remains stable when, at 6 s, the physical sensor is no more able to provide the measure of the yaw rate and it is replaced by the DVS which estimates the yaw rate.

6. Conclusions

A study on the use of VSs for fault tolerance in vehicle yaw control has been presented. Such a study is based on a new approach to virtual sensors design in which the VS is directly (DVS) derived from the data collected in a preliminary experiment. It has been shown that the use of data collected in a closed loop fashion

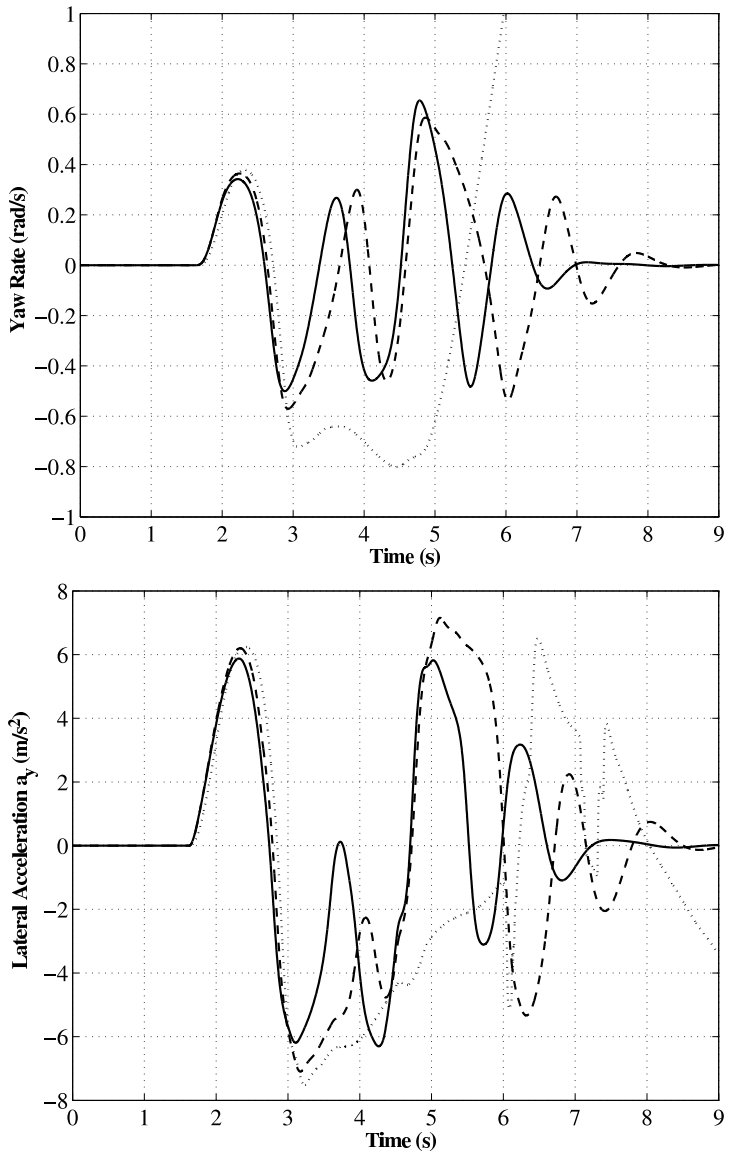

Figure 10. ISO double line change test at 100 km/h on wet road with vehicle mass increased by +200 kg w.r.t. nominal conditions. From top to bottom: vehicle yaw rate, vehicle lateral acceleration. Dotted line: uncontrolled vehicle, solid line: vehicle controlled with $(Q + \dot{\psi})$, dashed line: vehicle controlled with $(Q + DVS)$.

in the DVS design leads to improvements on the estimation performance and to a reduction of the number of needed measured variables, with respect to the case of data collected in open loop fashion. A deep analysis of the vehicle performance has been carried out when the DVS replaces the physical sensor. The simulation results are encouraging and suggest that the technology of DVSs can be effectively applied in the automotive context.

7. Acknowledgments

The work of L. Fagiano has been partly supported by the European Union Seventh Framework Programme (FP7/2007-2013) under grant agreement n. PIOF-GA-2009-252284 - Marie Curie project "Innovative Control, Identification and Estimation Methodologies for Sustainable Energy Technologies".

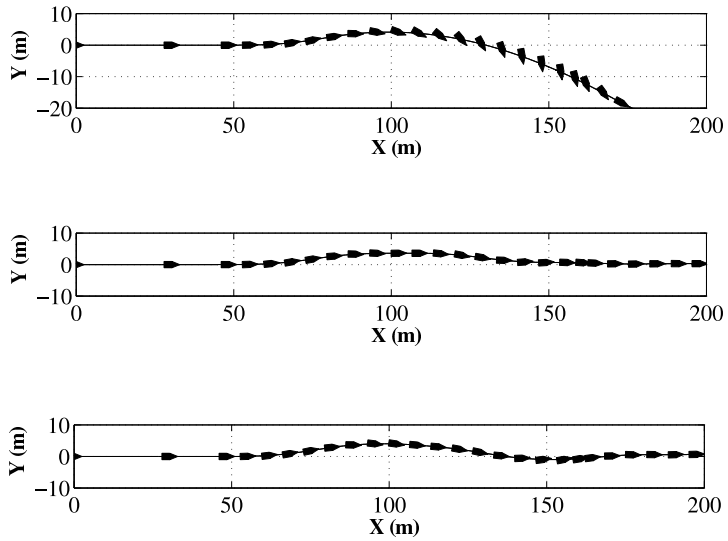

Figure 11. Vehicle trajectories obtained in the ISO double line change test at 100 km/h on wet road with vehicle mass increased by +200 kg w.r.t. nominal conditions. From top to bottom: uncontrolled vehicle, vehicle controlled with $(Q + \dot{\psi})$, vehicle controlled with $(Q + DVS)$.

References

[1] G.J. Forkenbrock, D. Elsasser, and B. OHara, *NHTSAs Light Vehicle Handling and ESC Effectiveness Research Program*, ESV Paper Number 05-0221 (2005).
[2] R. Rajamani *Vehicle Dynamics and Control*, Springer Verlag, 2005.
[3] P. Albertos and G.C. Goodwin, *Virtual Sensors for Control Applications*, Annual Reviews in Control 26 (2002), pp. 101–112.
[4] A. Hac and M.D. Simpson, *Estimation of Vehicle Side Slip Angle and Yaw Rate*, SAE Technical paper 2000-01-0696 (2000).
[5] G. Zhenhai, *Soft Sensor Application in Vehicle Yaw Rate Measurement Based on KALMAN Filter and Vehicle Dynamics*, in 6^{th} *IEEE Intelligent Transportation Systems Conference*, Shanghai, China, 2003, pp. 1352–1354.
[6] W. Chee, *Yaw Rate Estimation Using Two 1-Axis Accelerometers*, in *American Control Conference*, Portland, USA, 2005, pp. 423–428.
[7] M. Canale, L. Fagiano, F. Ruiz, and M. Signorile, *A study on the use of virtual sensors in vehicle control*, in *Proc. of the 47th IEEE Conference on Decision and Control*, Cancun, Mexico, 2008.
[8] M. Milanese, F. Ruiz, and M. Taragna, *Virtual sensors for linear dynamic systems: structure and identification*, in 3^{rd} *International IEEE Scientific Conference on Physics and Control (PhysCon 2007)*, Postdam, Germany, 2007.
[9] M. Milanese, C. Novara, K. Hsu, and K. Poolla, *Filter design from data: direct vs. two-step approaches*, in *American Control Conference*, Minneapolis, MN, 2006, pp. 4466–4470.
[10] L.R. Ray, *Nonlinear State and Tire Force Estimation for Advanced Vehicle Control*, IEEE Transactions on Control Systems Technology 3 (1995), pp. 117–124.
[11] H. Cherouat and S. Diop, *An Observer and an integrated braking/traction and steering control for a cornering vehicle*, in 24^{th} *American Control Conference*, Portland, USA, 2005, pp. 2212–2217.
[12] P. Kohen and M. Ecrick, *Active Steering - The BMW Approach Towards Modern Steering Technology*, in *SAE Technical Paper No. 2004-01-1105*, 2004.
[13] M. Morari and E. Zafiriou *Robust Process Control*, Prentice Hall, 1989.
[14] M. Canale, L. Fagiano, M. Milanese, and P. Borodani, *Robust vehicle yaw control using an active differential and IMC techniques*, Control Engineering Practice 15 (2007), pp. 923–941.
[15] M. Canale and L. Fagiano, *A robust IMC approach for stability control of 4WS vehicles*, Vehicle System Dynamics 46 (2008), pp. 991–1011.
[16] ———, *Comparing rear wheel steering and rear active differential approaches to vehicle yaw control*, Vehicle System Dynamics 48 (2009), pp. 529–549.
[17] A.T. Van Zanten, R. Erhart, and G. Pfaff, *VDC, The Vehicle Dynamics Control System of Bosch*, , in *SAE Technical Paper No. 95759* , 1995.
[18] A.T. Van Zanten, *Bosch ESP Systems: 5 Years of Experience*, in *SAE Technical Paper No. 2000-01-1633*, 2000.
[19] J. Ackermann and W. Sienel, *Robust Yaw Damping of Cars with Front and Rear Wheel Steering*, IEEE Trans. on Control Systems Technology 1 (1993), pp. 15–20.
[20] B.A. Güvenç, T. Bünte, and L. Güvenç, *Robust Two Degree-of-Freedom Vehicle Steering Controller Design*, IEEE Trans. on Control System Technology 12 (2004), pp. 627–636.
[21] G. Genta *Motor Vehicle Dynamics, II ed.*, World Scientific, 2003.
[22] S. Skogestad and I. Postlethwaite *Multivariable Feedback Control. 2^{nd} edition*, Wiley, 2005.
[23] M. Milanese, F. Ruiz, and M. Taragna, *Direct data-driven filter design for uncertain LTI systems with bounded noise*, Automatica 46 (2010), pp. 1773 – 1784.
[24] U. Al-Saggaf and G. Franklin, *An error bound for a discrete reduced order model of a linear multi-*

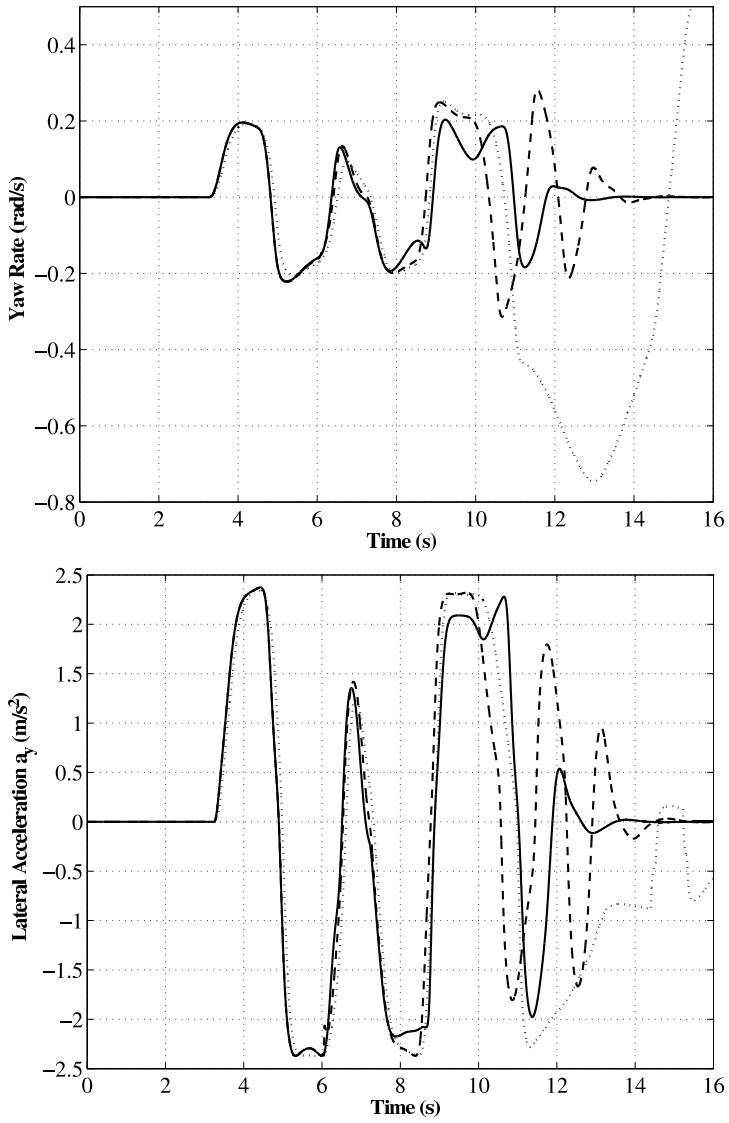

Figure 12. ISO double line change test at 50 km/h on iced road. From top to bottom: vehicle yaw rate, vehicle lateral acceleration. Dotted line: uncontrolled vehicle, solid line: vehicle controlled with $(Q + \dot{\psi})$, dashed line: vehicle controlled with $(Q + \dot{\psi})$ until 6 s when the fault occurs and then with $(Q + DVS)$.

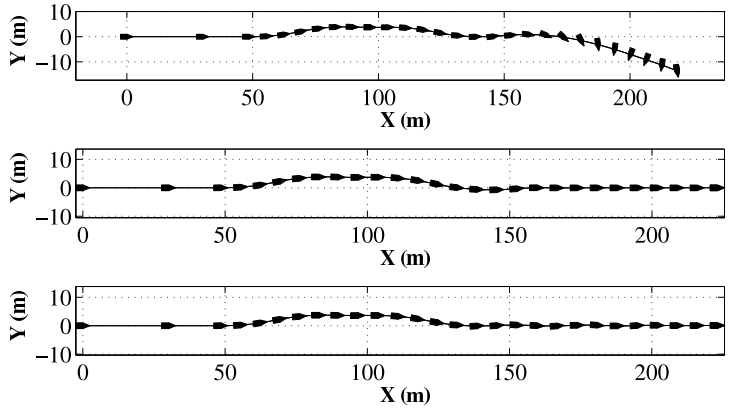

Figure 13. Vehicle trajectories obtained in the ISO double line change test at 50 km/h on iced road. From top to bottom: uncontrolled vehicle, vehicle controlled with $(Q + \dot{\psi})$, vehicle controlled with $(Q + \dot{\psi})$ until 6 s when the fault occurs and then with $(Q + DVS)$.

variable system, Automatic Control, IEEE Transactions on 32 (1987), pp. 815 – 819.